Revision 1 Word Count: 6318

Revision 1

Elucidating the natural-synthetic mismatch of $Pb^{2+}Te^{4+}O_3$: the redefinition of fairbankite to $Pb^{2+}_{12}(Te^{4+}O_3)_{11}(SO_4)$

OWEN P. MISSEN[1,2,*], MICHAEL S. RUMSEY[3], STUART J. MILLS[1], MATTHIAS WEIL[4], JENS NAJORKA[5], JOHN SPRATT[5], AND UWE KOLITSCH[6,7]

[1]Geosciences, Museums Victoria, GPO Box 666, Melbourne 3001, Victoria, Australia

[2]School of Earth, Atmosphere and Environment, Monash University, Clayton 3800, Victoria, Australia

[3] Department of Earth Sciences, Natural History Museum, Cromwell Road, London SW7 5BD, England, UK

[4]Institute for Chemical Technologies and Analytics, Division of Structural Chemistry, TU Vienna, Getreidemarkt 9/164-SC, A-1060 Vienna, Austria

[5]Department of Core Research Laboratories, Natural History Museum, Cromwell Road, London SW7 5BD, England, UK

[6]Department of Mineralogy and Petrography, Natural History Museum, Burgring 7, A-1010 Vienna, Austria

[7]Institute of Mineralogy and Crystallography, University of Vienna, Althanstr. 14, A-1090 Vienna, Austria

*Corresponding e-mail: omissen@museum.vic.gov.au

ABSTRACT

For four decades fairbankite was reported to have the formula $Pb^{2+}(Te^{4+}O_3)$, but repeated attempts to isolate fairbankite crystals for structural determination found only the visually similar cerussite and, more rarely, anglesite. The crystal-structure determination of fairbankite using single-crystal X-ray diffraction, supported by electron microprobe analysis and X-ray powder diffraction on the type specimen, has shown that fairbankite contains essential S, along with Pb, Te, and O. The chemical formula of fairbankite has been revised to $Pb^{2+}_{12}(Te^{4+}O_3)_{11}(SO_4)$. This change has been accepted by the IMA−CNMNC, Proposal 19-I. The crystal structure of fairbankite [space group *P*1 (no. 1); revised cell: a = 7.0205(3) Å, b = 10.6828(6) Å, c = 14.4916(8) Å, α = 75.161(5)°, β = 81.571(4)°, γ = 83.744(4)°, V = 1036.35(9) $Å^3$ and Z = 1] is the first atomic arrangement known to contain a $Te^{4+}_3O_9^{6-}$ non-cyclic, finite building unit. Fairbankite has an average structure, formed from a 3D framework of $Pb^{2+}O_n$ polyhedra, $Te^{4+}O_n$ polyhedra, and SO_4 tetrahedra in a 12:11:1 ratio. The stereoactive lone pairs of the Pb^{2+} and Te^{4+} cations are oriented into void space within the structure. Fairbankite contains two mixed sites statistically occupied by Te^{4+} and S^{6+} in approximately 4:1 and 1:4 ratios. These two sites possess Te in trigonal pyramidal geometry and S in tetrahedral geometry (with an additional O site to create tetrahedral SO_4 geometry for the S-dominant site). Six of the ten fully occupied Te^{4+} sites have Te^{4+} in trigonal pyramidal geometry, while four have Te^{4+} at the center of highly distorted $Te^{4+}O_4$ disphenoids. The disphenoids allow for the creation of two dimeric $Te^{4+}_2O_6^{4-}$ units in addition to the $Te^{4+}_3O_9^{6-}$ trimeric unit, which contains two disphenoids. All linkage between disphenoids and trigonal pyramids is *via* corner-linking. Secondary connectivity is *via* long Te–O and Pb–O bonds.

Keywords: lead tellurite; fairbankite; redefinition; crystal structure; tellurium oxysalt; average structure; Tombstone, Arizona, USA

This is the peer-reviewed, final accepted version for American Mineralogist, published by the Mineralogical Society of America.
The published version is subject to change. Cite as Authors (Year) Title. American Mineralogist, in press.
DOI: https://doi.org/10.2138/am-2020-7536. http://www.minsocam.org/

INTRODUCTION

A detailed description of synthetic compounds with the apparently simple formula $Pb^{2+}Te^{4+}O_3$ (monoclinic α-$Pb^{2+}Te^{4+}O_3$, tetragonal β-$Pb^{2+}Te^{4+}O_3$ and triclinic γ-$Pb^{2+}Te^{4+}O_3$) is given by Weil *et al.* (2018). A synthetic cubic form of $Pb^{2+}Te^{4+}O_3$ has also been reported (Gaitán *et al*., 1987) but no crystal structure is known and its identity is therefore dubious (Weil *et al.*, 2018). Neither of the two minerals with the reported formula $Pb^{2+}Te^{4+}O_3$ (plumbotellurite and fairbankite) showed unit-cell data matching the synthetic compounds. Data for the discredited (Burke, 2006) lead tellurite mineral 'dunhamite' (Fairbanks, 1946) is entirely lacking. Recently, Missen *et al.* (2019) demonstrated that plumbotellurite (Back, 1990) was incorrectly characterized and is in fact the natural analogue of synthetic α-$Pb^{2+}Te^{4+}O_3$ (Zavodnik *et al*., 2008), leaving only fairbankite as a mismatch with the two remaining synthetic compounds. Fairbankite was originally reported – without a crystal structure and on the basis of a wet-chemical analysis – as triclinic $Pb^{2+}Te^{4+}O_3$ by Williams (1979) from the Tombstone mining area, Arizona, USA. Williams (1979) suggested the unit-cell parameters a = 7.81, b = 7.11, c = 6.96 Å, α = 117.2°, β = 93.8° and γ = 93.4°, on the basis of X-ray rotation and Weissenberg techniques; an indexed X-ray powder diffraction pattern was also given. The Tombstone mining district is a series of former Ag–Pb–Mn mines and a rich locality for the discovery of Te-oxysalts, some of which have been recently reanalyzed by several of the present authors (see Table 1). In this paper we show that the crystal structure of fairbankite contains sulfate (SO_4) groups in addition to Pb, Te and O. The redefinition of fairbankite based on our updated analysis has been approved by the IMA–CNMNC, Proposal 19-I.

SPECIMEN DESCRIPTION

The Natural History Museum, London (NHM) type specimen of fairbankite (BM 1980,540; Figs. 1–3) also doubles as the former type specimen of 'oboyerite' (Williams, 1979), which is now designated as a 'dead type' for that mineral (Missen *et al*., 2019). The specimen contains fairbankite and winstanleyite, with the winstanleyite on the specimen misidentified as 'oboyerite' (Williams, 1979; Missen *et al*. 2019). Fairbankite was considered dubious on the sample for many years, as sampling from this type specimen had yielded only cerussite, or occasionally anglesite. Since Williams had also supplied other major museums with fairbankite "type" material (although he does not state any depository in his 1979 paper), we reinvestigated the fairbankite specimen in the collection of the National Museum of Natural History (Smithsonian), Washington, USA. Similar issues with official and non-official "type" material were experienced in the study of 'oboyerite' (Missen *et al*. 2019). Three crystals from the Smithsonian specimen fitting the description of fairbankite were sampled and studied by single-crystal X-ray diffraction (SXRD); all turned out to be cerussite. A careful visual investigation of the specimen revealed that the only further mineral phases on it were jarosite (matrix of the cerussite), opal (on jarosite), and rare yellow-green chlorargyrite. The observed assemblage is consistent with the description by Williams (1979) who had also noted that fairbankite is visually very similar to cerussite and anglesite. A further fairbankite specimen in the collection of the Muséum National d'Histoire Naturelle (Paris, France) could not be sampled because curator Cristiano Ferraris replied that "it is impossible to select crystals for [your] research; the samples are simply too small." (written comm. to U.K., March 2015). Therefore, whole-rock SEM mapping was undertaken to establish if the Natural History Museum (London) sample BM 1980,540 had any claim as a type specimen for fairbankite. During the analysis, we finally identified, apart from ample cerussite, crystals of a Pb–Te dominant mineral matching Williams' (1979) original

description (Figs. 1 and 2). The fairbankite forms a few nearly colorless, transparent crystals with indistinct morphology up to 200 μm across, lining some of the cavities on the specimen (Fig. 3). The specimen is a fractured piece of quartz gossan containing a box-work of cavities with morphologies suggestive of weathered-out primary sulfides, such as precursor primary minerals before the crystallization of secondary phases (Missen *et al*., 2020). The box-work cavities and fractures host, alongside fairbankite, a surprising variety of secondary minerals, including undifferentiated iron oxides/hydroxides, cerussite, chlorargyrite, jarosite, botryoidal 'opal', rodalquilarite [$H_3Fe^{3+}_2(Te^{4+}O_3)_4Cl$], poughite [$Fe^{3+}_2(Te^{4+}O_3)_2(SO_4)\cdot 3H_2O$] and possibly burckhardtite [$Pb^{2+}_2(Fe^{3+}Te^{6+})(AlSi_3O_8)O_6$] (Fig. 3).

CHEMISTRY

Quantitative chemical spot analyses (15) of a small fragment removed from the fairbankite type specimen and mounted in a probe block were performed on a Cameca SX100 electron microprobe (WDS mode, 20 kV, 20 nA, 1 μm beam diameter and PAP matrix correction) at the Imaging and Analysis Centre, Core Research Laboratories, NHM. The X-ray lines and standards used for element determination were: Si*K*α and Ca*K*α – wollastonite, S*K*α – barite, Mn*K*α – $MnTiO_3$, Cu*K*α and Fe*K*α – chalcopyrite, As*L*α – nickel arsenide, Se*L*α – lead selenide, Sb*L*α – Sb metal, Te*L*α – TeO_2 and Pb*M*α – vanadinite. A trace of SeO_2 was detected in one analysis, while other elements were sought, but not detected. The analytical data are presented in Table 2.

The empirical formula (based on 37 O anions *pfu*) is $Pb^{2+}_{12.17}Te^{4+}_{11.04}S_{0.92}Si_{0.04}O_{37}$. As all Te^{4+} sites have three close O neighbors (see below), the ideal end-member formula of fairbankite is $Pb^{2+}_{12}(Te^{4+}O_3)_{11}(SO_4)$, which requires PbO 59.33%, TeO_2 38.89%, and SO_3 1.77%, total 100.00 wt%.

Compared to Williams (1979), the chemical analysis totals have the significant advantage of being performed by EPMA rather than wet-chemical techniques. In particular, no correction for insoluble material was required in this study (cerussite comprised 13.0 wt% of the pre-normalized Williams (1979) total, sampled due to the close association of the two minerals on the specimen).

CRYSTALLOGRAPHY

X-ray powder diffraction

A large, slightly irregularly shaped (0.057 × 0.083 × 0.143 mm) fairbankite crystal, adjacent to, and from the same cavity as the crystal removed for chemical analysis was sampled from the type specimen (BM 1980,540) and attached to a non-diffracting amorphous-carbon fiber (10 μm diameter) glued to a glass support rod. This sample was mounted on a Rigaku Rapid II micro-diffractometer at the Natural History Museum, London, and a dataset was collected using Cu*K*α radiation (40 kV and 36 mA). Diffraction data were collected at ambient temperature using a 300 μm beam collimator, a primary graphite monochromator and a 2D curved image plate detector. A Gandolfi-type randomized sample movement was achieved by rotations on the φ and ω axes. The 2D diffraction data were converted to 1D patterns using the 2DP software (Rigaku). Observed d_{hkl} and reflection intensities were derived by profile-fitting using Highscore Plus software (Panalytical), although the dataset used was truncated at 60º 2θ due to poorly defined, low-intensity reflections at higher angles. High background resulted in lower than expected relative intensities for reflections found at less than 20° 2θ (d_{obs} greater than 4.46).

The unit-cell parameters of fairbankite were refined using Chekcell (Laugier & Bochu, 2004) from the powder data and are a = 7.027(3) Å, b = 10.680(3) Å, c = 14.493(6) Å, α = 75.14(2)°, β = 81.49(3)°, γ = 83.71(4)° and V = 1033(2) Å^3. These parameters are in

good agreement with the SXRD unit cell and with the pattern calculated from the structure using the PowderCell program (Kraus and Nolze, 1996). A comparison of observed and calculated reflections for the X-ray powder diffraction data is given in Table 3. Although the powder lines collected by Williams (1979) match reflections observed in this study, showing that the powder pattern he collected was from pure fairbankite, he indexed his data on a different triclinic cell with the unit-cell parameters a = 7.81, b = 7.11, c = 6.96 Å, α = 117.2°, β = 93.8°, γ = 93.4° and V = 342.4 Å^3. The unit-cell volume calculated from the crystal structure, 1036.35(9) Å^3, is approximately three times greater than that of Williams (1979).

Single Crystal X-ray Diffraction

The single crystal X-ray diffraction study was carried out at 293(2) K on an *Xcalibur* four-circle X-ray diffractometer equipped with an *EoS* area detector (both by Rigaku Oxford Diffraction) at the Natural History Museum, London, using graphite-monochromated Mo$K\alpha$ radiation (45 kV and 40 mA). The same large crystal used for PXRD measurements was used for single-crystal analysis.

Reflection intensities were integrated, corrected for Lorentz and polarization effects and converted to structure factors using the program CrysalisPro® (Rigaku Oxford Diffraction), finding 21374 reflections with an R_{int} of 0.0255. Due to the irregularly shaped crystal, a numerical (Gaussian) absorption correction was performed. The final structure of fairbankite was solved and refined in $P1$. Initially, the structure had been solved and refined in $P\bar{1}$ with unusually high atomic displacement parameters (ADPs) for oxygen atoms surrounding the one mixed Te/S site. This led us to redetermine the structure in the lower-symmetry space group $P1$, under consideration of an inversion twin with an approximate 1:1 ratio [refined ratio 0.527:0.473(10)]. The ADDSYM tool (checking for missed symmetry on the $P1$ model) as implemented in PLATON (Spek, 2009) did not indicate a necessary space group change. The $P1$ refinement doubled the number of sites compared to the initial $P\bar{1}$

174 structure solution, but resulted in a more satisfactory refinement (improved distances and
175 shapes of the polyhedra, lower residual electron densities, more reasonable U_{eq} values of the
176 O atoms), i.e. fairbankite contains $P\bar{1}$ pseudosymmetric elements but actually crystallizes in
177 $P1$. Structure solution in $P1$ was carried out using SHELXS-97 (Sheldrick, 2008), followed
178 by structural refinement using full-matrix least-squares implemented by SHELXL-2018/3
179 (Sheldrick, 2015), using neutral atomic scattering factors. The asymmetric unit of the $P1$
180 structure contains 12 Pb atoms, ten fully-occupied Te sites and two sites occupied by both Te
181 and S. The occupancies for Te and S in each of these two mixed sites were initially refined
182 freely, resulting in approximate 4:1 and 1:4 ratios. To obtain complete charge neutrality, the
183 occupancies were finally constrained to sum up to an overall charge of +2 for the mixed-
184 sites. No O sites were refined anisotropically as the anisotropic displacement parameters for
185 some O sites, although improved from the $P\bar{1}$ refinement, remained physically meaningless
186 ("non-positive-definite" character). It is worth noting that refining the O sites anisotropically
187 did not result in improved R indices.

188 Approximately 15 faint reflections were detected that indicated a very weakly
189 pronounced doubling of any one of the three unit-cell parameters. These reflections, e.g. at
190 *hkl* values of 1/2 0 2, 3/2 2 0 and 0 5/2 -3/2 (Fig. 4), did not have sufficient intensities to
191 allow for a refinement of the overall structure with one axis parameter doubled. More weak
192 reflections were present but only just above background. Hence, we refined an average
193 structure. Reflections with calculated F_{obs}/F_{calc} errors greater than 5.00 were omitted from the
194 final refinement. All atom positions and anisotropic displacement parameters (U^{ij}) for Pb, Te,
195 and S atoms were refined to final R_1 and wR_2 (all data) values of 0.0414 and 0.0641,
196 respectively. Further details of data collection and structure refinement are provided in
197 Supplementary Table 1. A summary of bond lengths is provided in Supplementary Table 2. A
198 bond-valence analysis is provided in Supplementary Table 3, using the parameters of

Krivovichev and Brown (2001) for Pb–O bonds, Mills and Christy (2013) for Te^{4+}–O bonds, and Gagné and Hawthorne (2015) for S–O bonds. Bond-valence sums for the two mixed sites were calculated based on the refined site occupancies for Te and S, although secondary bonds for these two sites were only attributed to the Te component.

Crystallographic data for fairbankite in the form of the Crystallographic Information File (CIF) been deposited with the Cambridge Crystallographic Data Centre, CCDC, 12 Union Road, Cambridge CB21EZ, UK. Copies of the data can be obtained free of charge on quoting the depository number CSD-2009504 (Fax: +44-1223-336-033; E-Mail: deposit@ccdc.cam.ac.uk, http://www.ccdc.cam.ac.uk).

Crystal-Structure Description

The crystal structure of fairbankite (Fig. 5) is formed from $Pb^{2+}O_n$ polyhedra, $Te^{4+}O_n$ polyhedra and SO_4 tetrahedra (one SO_4 tetrahedron to every eleven $Te^{4+}O_n$ units), forming a three-dimensional framework. The small channels within the framework are empty aside from the stereoactive lone pairs of Te^{4+} and Pb^{2+}. Our structure model describes an average structure due to the two mixed Te/S sites (Te11/S1 and S2/Te12), which are described below.

Both the Pb^{2+} and Te^{4+} cations display one-sided coordination environments. The coordination number of Pb varies from 5 (Pb3) to 9 (Pb12), with any O sites at greater distances than the nearest Te^{4+} cation to a Pb^{2+} cation not included in the Pb^{2+} coordination sphere (see Table 4). Bond-valence sums for Pb vary between 1.84 valence units (*vu*) for Pb3 and 2.07 *vu* for Pb12, showing a positive correlation between lower coordination by O and lower bond-valence. Te^{4+} coordination environments are either typical $Te^{4+}O_3$ trigonal pyramids (with Te–O bond lengths between 1.85 and 1.92 Å), or highly distorted $Te^{4+}O_4$ polyhedra. The Te1, Te2, Te4 and Te6 sites display distorted [3+1] disphenoidal coordination with three close primary bonds between 1.85 and 1.95 Å and one additional Te–O primary bond between 2.47 and 2.66 Å. These long primary bonds allow for the formation of three

distinct *soro* non-cyclic finite units (one $Te^{4+}{}_3O_9{}^{6-}$ trimer; Fig. 6a; and two $Te^{4+}{}_2O_6{}^{4-}$ dimers; Figs. 6b and c) through corner-sharing between one or two $Te^{4+}O_4$ disphenoids and one $Te^{4+}O_3$ trigonal pyramid. The $Te^{4+}{}_3O_9{}^{6-}$ trimer (Fig. 6a) is apparently unique amongst all known compounds, natural or synthetic (see below). All of the $Te^{4+}O_n$ polyhedra are linked to $Pb^{2+}O_n$ polyhedra by corner-linking. Most Te sites have three secondary bonds (see Table 5; Fig. 6), one of the most typical numbers of secondary bonds (Christy and Mills, 2013). Te secondary bonds (Figs. 6c and d) also provide further linkages to more distal O atoms, providing stability to the fairbankite framework, including one secondary bond formed between two of the participating sites in the new trimeric anion. The secondary bonds are rather short in some cases, only narrowly surpassing the usual 2.7 Å cut-off (Christy and Mills, 2013). The bond-valence sums for the Te sites vary between 3.82 (Te5) and 4.15 (Te6) *vu*, not including the distorted sums for the mixed Te/S sites, discussed in the next paragraph.

Fairbankite contains two mixed cation sites (Fig. 7), occupied by both Te (Te11 and Te12) and S (S1 and S2) in near 4:1 (Te11:S1; Fig. 7a) and 1:4 (Te12:S2; Fig. 7b) ratios, with the ratio of free variables for site occupancies refined to 0.807:0.193(4) and 0.193:0.807(4), respectively. The closest O sites to the mixed sites have average lengths between those typically found for S^{6+}–O and short Te^{4+}–O bonds. Typical S^{6+}–O bond lengths average 1.481 Å (value calculated from bond-valence parameters of Gagné and Hawthorne, 2015), while Te^{4+}–O bond lengths are typically 1.911 ± 0.077 Å (Mills and Christy, 2013). The average short bond length for the Te-dominant Te11/S1–O site is 1.78 Å, i.e. closer to the average length for Te^{4+}–O bonds, while for the S-dominant S2/Te12 site, the reverse is true, with an average of 1.55 Å: closer to average S^{6+}–O bonds. The O37 site – essentially the fourth bond for S to complete a SO_4 tetrahedron – is present on the S2/Te12 (S-rich) site, and does not have an equivalent on the Te11/S1 site – for this reason, the Te12–O37 component of the S2/Te12–O37 bond was not included in bond-valence calculations. 1/5

of an O site is below the electron counts of the highest *Q*-residual electron density peaks close to heavy-atom sites in the structure (2.33 electrons). Thus, although ideally O37 would have an occupancy of 0.807(4), and an equivalent O ligand with an occupancy of 0.193(4) for the Te11/S1 site would be present, this detail cannot be accurately refined. Therefore, for charge balance O37 was refined as fully occupied. The bond-valence sum calculated for the Te11/S1 site is 4.26 *vu*, while it is 5.61 *vu* for the S2/Te12 site – i.e. in each case closer to the value expected for the dominant cation. The local S2 position is expected to be moved ~0.1 Å further from O37 and closer to O34, O35 and O36, so that the average S2–O distance is ~1.48 Å. The local Te11 position would ideally move ~0.1 Å further away from O31, O32 and O33, so that the average Te11–O distance is ~1.91 Å. The minority positions of Te12 and S1 would be expected to move in the opposite directions to the majority sites, however, this detail cannot easily be refined due to constraints imposed by the average structure.

Relationship to other Tellurium Oxysalt Structures

Fairbankite is not a fourth polymorph of $Pb^{2+}Te^{4+}O_3$, instead (as discussed) it contains essential SO_4 groups. The correct formula for fairbankite may be compared with those of the minerals adanite, $Pb^{2+}_2(Te^{4+}O_3)(SO_4)$ (Kampf *et al.* 2020) and northstarite, $Pb^{2+}_6(Te^{4+}O_3)_5(S_2O_3^{2-})$, which instead contains a thiosulfate ($S_2O_3^{2-}$) anion (Kampf *et al.* 2019). Schieffelinite $[Pb_{10}Te^{6+}_6O_{20}(OH)_{14}(SO_4)(H_2O)_5]$ also displays some similarities to fairbankite, although schieffelinite contains hexavalent Te and additionally contains both OH anions and H_2O groups (Kampf *et al.* 2012).

Fairbankite contains isolated *neso* tellurite $(Te^{4+}O_3)^{2-}$ groups, isolated *soro* dimeric non-cyclic finite ($Te^{4+}_2O_6^{4-}$) groups and isolated *soro* trimeric non-cyclic finite ($Te^{4+}_3O_9^{6-}$) units – all of which are part of a larger structural group (Christy *et al.* 2016a). The minerals juabite, $CaCu_{10}(Te^{4+}O_3)_4(AsO_4)_4(OH)_2{\cdot}4H_2O$ (Roberts *et al.* 1997; Kampf and Mills, 2011) and rodalquilarite (Kampf and Mills, 2011) have *neso* units as part of a larger structural layer,

while moctezumite, $Pb(UO_2)(Te^{4+}O_3)_2$ (Swihart *et al.* 1993), mroseite, $CaTe^{4+}(CO_3)O_2$ (Fischer *et al.* 1975) and poughite (Kampf and Mills, 2011) have *soro* dimers as part of a structural framework. Fairbankite is the first example of any compound to contain s*oro* $Te_m^{4+}O_n$ non-cyclic finite units for which $m > 2$. The crystal structure of synthetic $Dy_2Te_3O_9$ (Meier *et al*. 2009) contains trimeric units if a Te–O bond-length cutoff of 2.65 Å is applied. There is, however, a fifth Te–O bond in the primary coordination sphere at 2.654 Å (0.18 vu bond-strength) linking the trimeric units into infinite complex chains formed from $Te^{4+}O_3$ trigonal pyramids, $Te^{4+}O_4$ disphenoids and $Te^{4+}O_5$ polyhedra. Thus, $Dy_2Te_3O_9$ should be classified as an inotellurite (Meier *et al*. 2009). Interestingly, of the six minerals (including fairbankite) containing *neso* or *soro* Te^{4+}–O units as part of a larger layer or framework structure, both rodalquilarite and poughite are also associated with fairbankite on specimen BM 1980,540. This association probably indicates that the physio-environmental conditions, and not just chemistry, can have a bearing on the Te–O structural units (and their polymerization) found in a (local) mineral assemblage (Christy *et al*. 2016a,b).

IMPLICATIONS

The combined studies of plumbotellurite (Missen *et al*. 2019) and fairbankite unequivocally align our understanding of the synthetic $Pb^{2+}Te^{4+}O_3$ materials with occurrences in Nature. Until these studies, the complexity of natural mineralogical phases has led material scientists, crystallographers, geologists and mineralogists ‘up the garden path’, believing that there might be 5 or 6 different polymorphs of what is stoichiometrically a simple chemical composition. Additionally, the redefinition of fairbankite has resulted in the description of a previously unknown sorotellurite anion.

Determining that plumbotellurite is α-$Pb^{2+}Te^{4+}O_3$ and that fairbankite is not a polymorph of $Pb^{2+}Te^{4+}O_3$ shows that our understanding of synthetic compounds matches

what we see in Nature, underscoring the importance of accurate characterization of minerals and retention of type samples. Minerals whose definitions are based on wet chemistry or other bulk techniques must be reinvestigated *de rigueur*. The most recent decades in mineralogical research have resulted in a greater appreciation in how micro- and even nano-scale intergrowths of minerals inform macro-scale properties of mineral assemblages, an approach which relies upon accurate characterization of rare phases (Kampf *et al*., 2017; Missen *et al*., 2019). In many cases secondary (Te) minerals remain poorly characterized (Christy *et al*., 2016a), despite the tendency for these minerals to have unique structures which have never been synthesized. Secondary (Te) minerals are a rich natural source of new structural diversity, with this study alone implying that two $Pb^{2+}Te^{4+}O_3$ polymorphs are yet to be discovered in Nature.

Finally, it should also be noted that elucidating the structure of fairbankite shows the importance of a crystal structure during naming and characterization. Sulfate was not detected in the original wet chemical analysis of fairbankite, and without a crystal structure to show the mismatch, its presence was not noticed until four decades later, confirmed herein by modern EPMA and SXRD analysis.

ACKNOWLEDGEMENTS

We thank two anonymous reviewers and the technical editor for their insightful comments, which improved the manuscript. This study has been partly funded by The Ian Potter Foundation grant 'tracking tellurium' to SJM. Microprobe work was funded through Natural Environment Research Council grant NE/M010848/1 'Tellurium and Selenium Cycling and Supply' to Chris J. Stanley (Natural History Museum, London). Support funding has also been provided to OPM by an Australian Government Research Training Program (RTP) Scholarship, a Monash Graduate Excellence Scholarship (MGES) and a Robert

Blackwood Monash-Museums Victoria scholarship. Mark D. Welch (Natural History Museum, London) is thanked for his assistance with the absorption correction processes. We acknowledge Joël Brugger (Monash University) for his insightful comments. Paul W. Pohwat (Smithsonian Institution) and Cristiano Ferraris (MNHN Paris) are thanked for their help with providing catalogued fairbankite specimens.

REFERENCES CITED

Back, M.E. (1990) A Study of Tellurite Minerals: Their Physical and Chemical Data Compatibility, and Structural Crystallography. MSc Thesis, University of Toronto, Canada.

Bindi, L. and Cipriani, C. (2003) The crystal structure of winstanleyite, $TiTe_3O_8$, from the Grand Central Mine, Tombstone, Arizona. Canadian Mineralogist, 41, 1469–1473.

Burke, E.A.J. (2006) A mass discreditation of GQN minerals. Canadian Mineralogist, 44, 1557–1560.

Cooper, M.A., Hawthorne, F.C., and Back, M.E. (2008) The crystal structure of khinite and polytypism in khinite and parakhinite. Mineralogical Magazine, 72, 763–770.

Christy, A.G. and Mills, S.J. (2013) Effect of lone-pair stereoactivity on polyhedral volume and structural flexibility: application to $Te^{IV}O_6$ octahedra. Acta Crystallographica, B69, 446–456.

Christy, A.G., Mills, S.J., and Kampf, A.R. (2016a) A review of the structural architecture of tellurium oxycompounds. Mineralogical Magazine, 80, 415–545.

Christy, A.G., Mills, S.J., Kampf, A.R., Housley, R.M., Thorne, B., and Marty, J. (2016b) The relationship between mineral composition, crystal structure and paragenetic sequence: the case of secondary Te mineralization at Otto Mountain, California, USA. Mineralogical Magazine, 80, 291–310.

Fairbanks, E.E. (1946) The punched card identification of ore minerals. Economic Geology, 41, 761–768.

Fischer, R., Pertlik, F., and Zemann, J. (1975) The crystal structure of mroseite, $CaTeO_2(CO_3)$. Canadian Mineralogist, 13, 383–387.

Gagné, O.C. and Hawthorne, F.C. (2015) Comprehensive derivation of bond-valence parameters for ion pairs involving oxygen. Acta Crystallographica, B71, 562–578.

Gaitán, M., Jerez, A., Noguerales, P., Pico, C., and Veiga, M. (1987) New Methods of synthesis of mixed oxides of Te and Pb: characterization of the new phases $PbTeO_3$ (cubic) and $PbTeO_4$ (orthorhombic). Synthesis and Reactivity in Inorganic and Metal-Organic Chemistry, 17, 479–490.

Hawthorne, F.C., Cooper, M.A., and Back, M.E. (2009) Khinite-4*O* [= khinite] and khinite-3*T* [= parakhinite]. Canadian Mineralogist, 47, 473–476.

Kampf, A.R., Housley, R.M., Mills, S.J., Marty, J., and Thorne, B. (2010) Lead-tellurium oxysalts from Otto Mountain near Baker, California: I. Ottoite, Pb_2TeO_5, a new mineral with chains of tellurate octahedra. American Mineralogist, 95, 1329–1336.

Kampf, A.R. and Mills, S.J. (2011) The role of hydrogen in tellurites: crystal structure refinements of juabite, poughite and rodalquilarite. Journal of Geosciences, 56, 235–247.

Kampf, A.R., Mills, S.J., Housley, R.M., Rumsey, M.S., and Spratt, J. (2012) Lead-tellurium oxysalts from Otto Mountain near Baker, California: VII. Chromschieffelinite, $Pb_{10}Te_6O_{20}(OH)_{14}(CrO_4)(H_2O)_5$, the chromate analog of schieffelinite. American Mineralogist, 97, 212–219.

Kampf, A.R., Mills, S.J., and Rumsey, M.S. (2017) The discreditation of girdite. Mineralogical Magazine, 81, 1125–1128.

Kampf A.R., Housley R.M., and Rossman G.R. (2019) Northstarite, IMA 2019-031. CNMNC Newsletter No. 51; Mineralogical Magazine, 83, 758, doi: 10.1180/mgm.2019.58.

Kampf, A.R., Housley, R.M., Rossman, G.R., Yang, H., and Downs, R.T. (2020) Adanite, IMA 2019-088. CNMNC Newsletter No. 53; Mineralogical Magazine, 84, 160, doi: 10.1180/mgm.2020.5.

Kraus, W. and Nolze, G. (1996) POWDER CELL—a program for the representation and manipulation of crystal structures and calculation of the resulting X-ray powder patterns. Journal of Applied Crystallography, 29, 301–303.

Krivovichev, S.V. and Brown, I.D. (2001) Are the compressive effects of encapsulation an artifact of the bond valence parameters? Zeitschrift für Kristallographie, 216, 245–247.

Laugier, J. and Bochu, B. (2004) Chekcell: Graphical powder indexing cell and space group assignment software, http://www.ccp14.ac.uk/tutorial/lmgp/.

Meier, S.F., Höss, P., and Schleid, T. (2009) $Dy_2Te_3O_9$: Der erste Vertreter von Lanthanoid(III)-Oxotelluraten der Zusammensetzung $M_2Te_3O_9$. Zeitschrift für anorganische und allgemeine Chemie, 635, 768–775 (in German).

Mills, S.J. and Christy, A.G. (2013) Revised values of the bond-valence parameters for Te^{IV}–O, Te^{VI}–O and Te^{IV}–Cl. Acta Crystallographica, B69, 145–149.

Missen, O.P., Rumsey, M.S., Kampf, A.R., Mills, S.J., Back, M.E., and Spratt, J. (2019) The discreditation of oboyerite and a note on the crystal structure of plumbotellurite. Mineralogical Magazine, 83, 791–797.

Missen, O.P., Ram, R., Mills, S.J., Etschmann, B., Reith, F., Shuster, J., Smith, D.J. and Brugger, J. (2020) Love is in the Earth: a review of tellurium (bio)geochemistry in surface environments. Earth-Science Reviews, 204, 103150.

Pertlik, F. (1972) Der Strukturtyp von Emmonsit, $\{Fe_2[TeO_3]_3 \cdot H_2O\} \cdot xH_2O$ (x = 0−1). Tschermaks mineralogische und petrographische Mitteilungen, 18, 157–168 (in German).

Roberts, A.C., Gault, R.A., Jensen, M.C., Criddle, A.J., and Moffatt, E.A. (1997) Juabite, $Cu_5(Te^{6+}O_4)_2(As^{5+}O_4)_2 \cdot 3H_2O$, a new mineral species from the Centennial Eureka mine, Juab County, Utah. Mineralogical Magazine, 61, 139–144.

Sheldrick, G.M. (2008) A short history of *SHELX*. Acta Crystallographica, A64, 112-122.

Sheldrick, G.M. (2015) Crystal structure refinement with *SHELXL*. Acta Crystallographica, C71, 3–8.

Spek, A.L. (2009) Structure validation in chemical crystallography. Acta Crystallographica, D65, 148–155.

Swihart, G.H., Sen Gupta, P.K., Schlemper, E.O., Back, M.E., and Gaines, R.V. (1993) The crystal structure of moctezumite $[PbUO_2][TeO_3]_2$. American Mineralogist, 78, 835–839.

Tait, K.T., DiCecco, V., Ball, N.A., Hawthorne, F.C., and Kampf, A.R. (2015) Backite, $Pb_2Al(TeO_6)Cl$, a new tellurate mineral from the Grand Central mine, Tombstone Hills, Cochise County, Arizona: description and crystal structure. Canadian Mineralogist, 52, 935–942.

Weil, M. and Shirkhanlou, M. (2017) Incorporation of Sulfate or Selenate Groups into Oxotellurates (IV): II. Compounds with Divalent Lead. Zeitschrift für anorganische und allgemeine Chemie, 643, 757–765.

Weil, M., Shirkhanlou, M., Füglein, E., and Libowitzky, E. (2018) Determination of the Correct Composition of "Hydrous Lead(II) Oxotellurate(IV)" as $PbTeO_3$, Crystallizing as a New Polymorph. Crystals, 8, 51.

Williams, S.A. (1978) Khinite, parakhinite, and dugganite, three new tellurates from Tombstone. Arizona. American Mineralogist, 63, 1016–10l9.

Williams, S.A. (1979) Girdite, oboyerite, fairbankite, and winstanleyite, four new tellurium minerals from Tombstone, Arizona. Mineralogical Magazine, 43, 453–457.

Williams, S.A. (1980) Schieffelinite, a new lead tellurate-sulphate from Tombstone, Arizona. Mineralogical Magazine, 43, 771–773.

Zavodnik, V.E., Ivanov, S.A., and Stash, A.I. (2008) α-Lead tellurite from single-crystal data. Acta Crystallographica, E64, i16.

431 **TABLES**

432 **Table 1:** Fairbankite and related Te–O minerals by locality (Tombstone area, Arizona, USA) and chemical composition

433

Mineral	Status	Formula	Year described	Comment	Type locality	Reference(s)
Tombstone area Te–O minerals						
Backite	Valid	$Pb^{2+}{}_2AlTe^{6+}O_6Cl$	2015	Unique chemical composition	Grand Central Mine	Tait *et al*. (2015)
Dugganite	Valid	$Pb^{2+}{}_3Zn_3(AsO_4)_2$-$(Te^{6+}O_6)$	1978	Relatively common in Tombstone area	Silver Plume Mine	Williams (1978)
Emmonsite	Valid	$Fe^{3+}{}_2(Te^{4+}O_3)_3$-$\cdot 2H_2O$	1885	One of the most common secondary Te minerals	Tombstone area – unclear which mine	Pertlik (1972)
Fairbankite	Valid	$Pb^{2+}{}_{12}(Te^{4+}O_3)_{11}(SO_4)$	1979	Very rare	Grand Central Mine	Williams (1979) and present study
'Girdite'	Discredited	n/a	1979	Discredited as a mixture of ottoite and plumbotellurite	Joe Mine	Williams (1979); Kampf *et al*. (2017)
Khinite	Valid	$Pb^{2+}Cu_3(Te^{6+}O_6)$-$(OH)_2$	1978	Common at Otto Mountain, CA, USA	Old Guard Mine	Williams (1978); Cooper *et al*. (2008)
'Oboyerite'	Discredited	n/a	1979	Discredited as a mixture of ottoite and plumbotellurite	Grand Central Mine	Williams (1979); Missen *et al*. (2019)
'Parakhinite'	Discredited	n/a	1978	Discredited as 3*T* polytype of khinite	Silver Plume Mine	Williams (1978); Hawthorne *et al*. (2009)
Schieffelinite	Valid	$Pb^{2+}{}_{10}Te^{6+}{}_6O_{20}(OH)_{14}$-$(SO_4)\cdot 5H_2O$	1979	Only hydrated Pb–Te–S–O mineral	Joe Mine	Williams (1980); Kampf *et al*. (2012)
Winstanleyite	Valid	$TiTe^{4+}{}_3O_8$	1979	Only Ti-containing Te-oxysalt	Grand Central Mine	Williams (1979); Bindi and Cipriani (2003)

This is the peer-reviewed, final accepted version for American Mineralogist, published by the Mineralogical Society of America.
The published version is subject to change. Cite as Authors (Year) Title. American Mineralogist, in press.
DOI: https://doi.org/10.2138/am-2020-7536. http://www.minsocam.org/

Related Pb–Te(–S)–O minerals						
Adanite	Valid	$Pb^{2+}{}_2(Te^{4+}O_3)(SO_4)$	2019	First known as a synthetic	North Star Mine, Utah, USA	Weil and Shirkhanlou (2017); Kampf *et al*. (2020)
'Dunhamite'	Discredited	n/a	1946	Discredited as '$PbTe^{4+}O_3$' due to insufficient data	Hilltop Mine, New Mexico, USA	Fairbanks (1946)
Northstarite	Valid	$Pb^{2+}{}_6(Te^{4+}O_3)_5(S_2O_3)$	2019	Unique chemical composition	North Star Mine, Utah, USA	Kampf *et al*. (2019)
Ottoite	Valid	$Pb^{2+}{}_2Te^{6+}O_5$	2010	First new mineral described from Otto Mountain	Otto Mountain mines, California, USA	Kampf *et al*. (2010)
Plumbotellurite	Valid	$Pb^{2+}Te^{4+}O_3$	1982	Monoclinic α-$Pb^{2+}Te^{4+}O_3$	Zhana-Tyube Au deposit, Kazakhstan	Back (1990); Zavodnik *et al*. (2008); Missen *et al*. (2019)

435 **Table 2:** EPMA data for the fairbankite specimen, including Williams' (1979) analysis for
436 comparison

	Type specimen (BM 1980,540) (15 analyses)				Williams' (1979) analysis
Oxide wt%	Average	Min	Max	St. Dev.	Average
SiO_2	0.05	0.0	0.14	0.05	
SO_3	1.61	1.23	1.92	0.18	-
TeO_2	38.62	37.45	39.62	0.66	36.4
PbO	59.51	58.13	61.04	0.83	50.9
$PbCO_3$*	-	-	-	-	13.0
Total	99.79				100.3

437
438 * $PbCO_3$ was noted as an insoluble contaminant.

439

This is the peer-reviewed, final accepted version for American Mineralogist, published by the Mineralogical Society of America.
The published version is subject to change. Cite as Authors (Year) Title. American Mineralogist, in press.
DOI: https://doi.org/10.2138/am-2020-7536. http://www.minsocam.org/

Table 3. X-ray powder diffraction data for fairbankite

<dt indicates reflection intensity was indistinguishable from background, n/a is not applicable.

Williams (1979)		This study		Simulated from crystal structure model		
I_{obs}	d_{obs}	I_{obs}	d_{obs}	d_{calc}	I_{calc}	*h k l*
<dt	n/a	4	5.212	5.204, 5.202	2, 5	1 1 2, 0 -1 2
20	5.150	<dt	n/a	5.149	5	0 2 0
20	4.652	7	4.673	4.674	10	0 1 3
10	3.561	3	3.569	3.567	5	0 1 4
100	3.265	100	3.268	3.264	100	-1 -2 2
60	3.148	82	3.151	3.151	92	0 3 3
60	3.098	49	3.105	3.102	83	-2 1 1
50	3.020	50	3.025	3.022	64	2 2 2
60	2.828	34	2.830	2.830	53	1 -3 1
50	2.516	34	2.520	2.520	36	-1 1 5
30	2.076	22	2.079	2.078	27	1 5 1
20	2.052	12	2.055	2.054	15	3 -1 3
30	1.944	26, 25	1.948, 1.947	1.948, 1.943	16, 15	1 3 7, 0 -2 6
20	1.920	35	1.923	1.922	18	-3 -1 3
20	1.825	16	1.825	1.826	14	-2 4 4
20	1.789	29	1.788	1.786	11	3 4 0
20	1.777	19	1.777	1.777	11	2 5 5
20	1.753	19	1.752	1.751	8	4 1 1
20	1.731	18	1.731	1.732	11	0 -5 3
10	1.671	11	1.670	1.672	10	-1 6 2
10	1.656	14	1.658	1.658	6	3 -4 0
20	1.632	18	1.632	1.632	8	-2 -4 4
10	1.585	11	1.584	1.586, 1.585, 1.584	2, 4, 1	2 -3 6, 0 1 9, 4 2 5
20	1.574	18	1.576	1.577, 1.575	6, 7	-2 -1 7, 0 6 6
10	1.552	10	1.551	1.551	5	-4 2 2
10	1.537	8	1.537	1.538	7	-1 4 8

This is the peer-reviewed, final accepted version for American Mineralogist, published by the Mineralogical Society of America.
The published version is subject to change. Cite as Authors (Year) Title. American Mineralogist, in press.
DOI: https://doi.org/10.2138/am-2020-7536. http://www.minsocam.org/

Table 4: Summary of Pb bonding in fairbankite with bond lengths in Å and bond valences in valence units (*vu*)
Secondary bonds cut off at the minimum Pb–*M* distance (where *M* represents any non O atom).

Pb center number	Pb center overall formula	Number of bonds < 3 Å	Number of bonds > 3 Å	Average <Pb–O> bond length	Overall <Pb–O> bond valence
Pb1	$Pb^{2+}O_7$	6	1	2.70	1.98
Pb2	$Pb^{2+}O_7$	6	1	2.67	1.98
Pb3	$Pb^{2+}O_5$	5	0	2.47	1.84
Pb4	$Pb^{2+}O_6$	6	0	2.55	1.87
Pb5	$Pb^{2+}O_6$	5	1	2.62	2.01
Pb6	$Pb^{2+}O_8$	4	4	2.82	1.98
Pb7	$Pb^{2+}O_7$	6	1	2.61	2.04
Pb8	$Pb^{2+}O_7$	7	0	2.61	1.95
Pb9	$Pb^{2+}O_7$	7	0	2.61	1.99
Pb10	$Pb^{2+}O_8$	6	2	2.75	2.01
Pb11	$Pb^{2+}O_8$	6	2	2.78	2.05
Pb12	$Pb^{2+}O_9$	5	4	2.86	2.07
Average	**$Pb^{2+}O_{7.08}$**	**5.75**	**1.33**	**2.67**	**1.98**

This is the peer-reviewed, final accepted version for American Mineralogist, published by the Mineralogical Society of America.
The published version is subject to change. Cite as Authors (Year) Title. American Mineralogist, in press.
DOI: https://doi.org/10.2138/am-2020-7536. http://www.minsocam.org/

Table 5: Summary of Te bonding in fairbankite with bond lengths in Å and bond valences in valence units (*vu*)
Secondary bonds cut off at 3.5 Å, following Christy and Mills (2013).
NB: The two mixed sites and their pertinent values are italicized. Te11/S1 site is Te-dominant, with a Te:S ratio of 0.807:0.193(4) and the S2/Te12 site is S-dominant, with the inverse ratio. Neither site is included in the calculation of overall averages.

Te center number	Te center overall formula	Number of primary bonds	<Te–O> primary bond length (Å)	<Te–O> primary bond valence (*vu*)	Number of secondary bonds	<Te–O> secondary bond length (Å)	<Te–O> secondary bond valence (*vu*)	Overall <Te–O> bond valence
Te1	$Te^{4+}O_6$	4	2.08	3.77	2	3.09	0.16	3.93
Te2	$Te^{4+}O_6$	4	2.08	3.77	2	2.97	0.19	3.96
Te3	$Te^{4+}O_5$	3	1.88	3.67	2	2.86	0.24	3.91
Te4	$Te^{4+}O_6$	4	2.05	3.67	2	2.92	0.20	3.87
Te5	$Te^{4+}O_6$	3	1.90	3.51	3	2.91	0.31	3.82
Te6	$Te^{4+}O_6$	4	2.04	4.06	2	3.20	0.10	4.15
Te7	$Te^{4+}O_6$	3	1.88	3.66	3	2.94	0.31	3.97
Te8	$Te^{4+}O_6$	3	1.89	3.56	3	2.94	0.28	3.84
Te9	$Te^{4+}O_6$	3	1.87	3.71	3	3.08	0.19	3.90
Te10	$Te^{4+}O_5$	3	1.88	3.68	2	2.88	0.21	3.90
Te11/S1	*$Te^{4+}O_5$*	*3*	*1.78*	*4.16*	*2*	*3.14*	*0.10*	*4.26*
S2/Te12	*$Te^{4+}O_4$*	*3*	*1.55*	*4.12*	*1*	*3.19*	*0.01*	*4.13*
Average	**$Te^{4+}O_{5.80}$**	**3.40**	**1.95**	**3.71**	**2.40**	**2.98**	**0.22**	**3.93**

452 **FIGURES AND CAPTIONS**

453

454 **Figure 1:** A backscatter whole-rock SEM image of the fairbankite type specimen (BM
455 1980,540), showing paragenetic relationships between the minerals – fairbankite forms early
456 in this secondary mineral assemblage. Abbreviations: Fbk (fairbankite), Pgh (poughite), Rdq
457 (rodalquilarite), Jrs (jarosite), Chl (chlorargyrite), and Opl (opal).

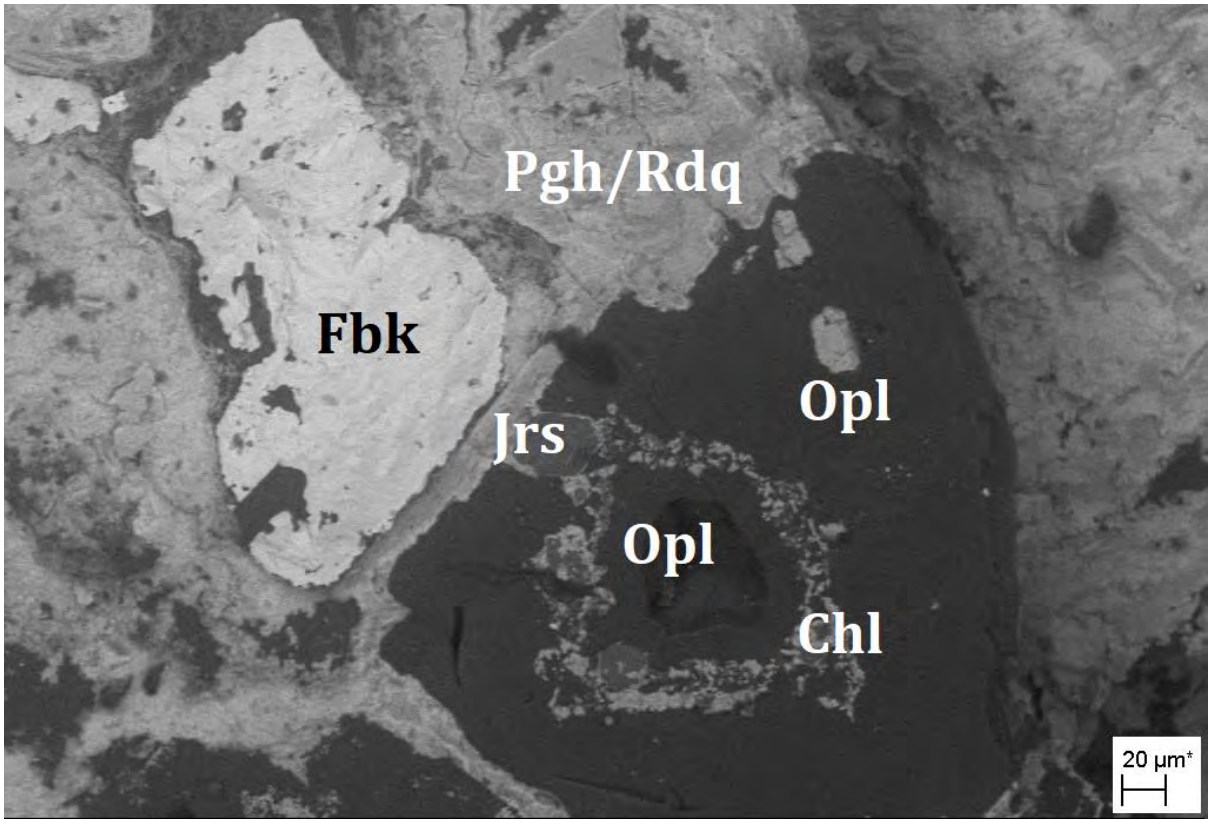

458

459

460 **Figure 2:** This backscatter-electron whole-rock SEM image of an area on the fairbankite type
461 specimen (BM 1980,540) shows that the visually similar fairbankite and cerussite are
462 texturally different (fairbankite appears smoother, cerussite more hackly), despite their
463 similar contrast in backscatter mode.

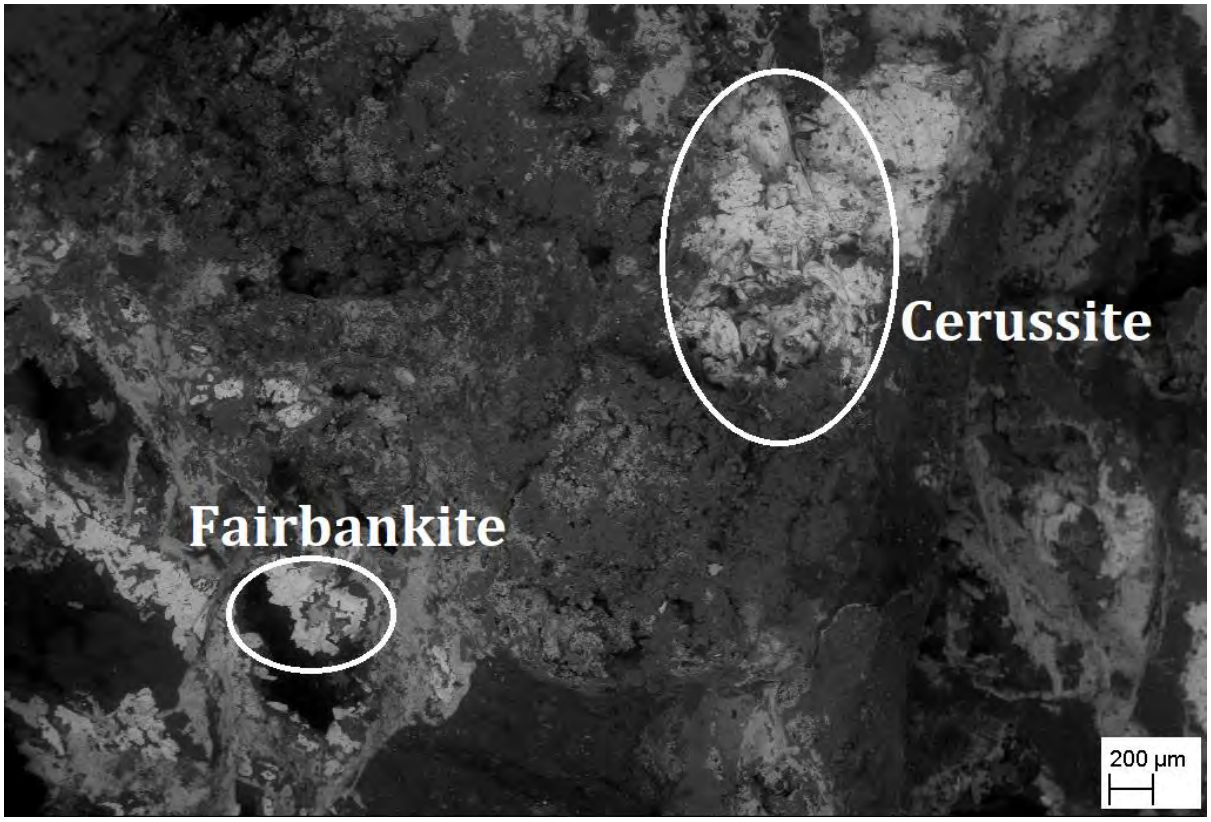

464

465

This is the peer-reviewed, final accepted version for American Mineralogist, published by the Mineralogical Society of America.
The published version is subject to change. Cite as Authors (Year) Title. American Mineralogist, in press.
DOI: https://doi.org/10.2138/am-2020-7536. http://www.minsocam.org/

466 **Figure 3:** Optical images of the fairbankite type specimen BM 1980,540. Image (a) shows
467 the slightly cream-coloured fairbankite crystals in the center of the image, surrounded in the
468 gossan by brown iron oxide/hydroxides, yellow-brown jarosite, minor brighter yellow
469 poughite, grey quartz, white-grey cerussite, flecks of green rodalquilarite and barely
470 discernable pinkish-grey chlorargyrite. A cavity lined entirely with late-stage 'opal' is visible
471 to the bottom left. Image (b) shows the fairbankite crystals within the vug atop aggregates of
472 yellow jarosite, with opal rimming some of the vug and some grey-pink chlorargyrite grains.
473 The crystal in the center of the image is the largest fairbankite crystal currently known
474 (approaching 0.5 mm in length).

475

476

This is the peer-reviewed, final accepted version for American Mineralogist, published by the Mineralogical Society of America.
The published version is subject to change. Cite as Authors (Year) Title. American Mineralogist, in press.
DOI: https://doi.org/10.2138/am-2020-7536. http://www.minsocam.org/

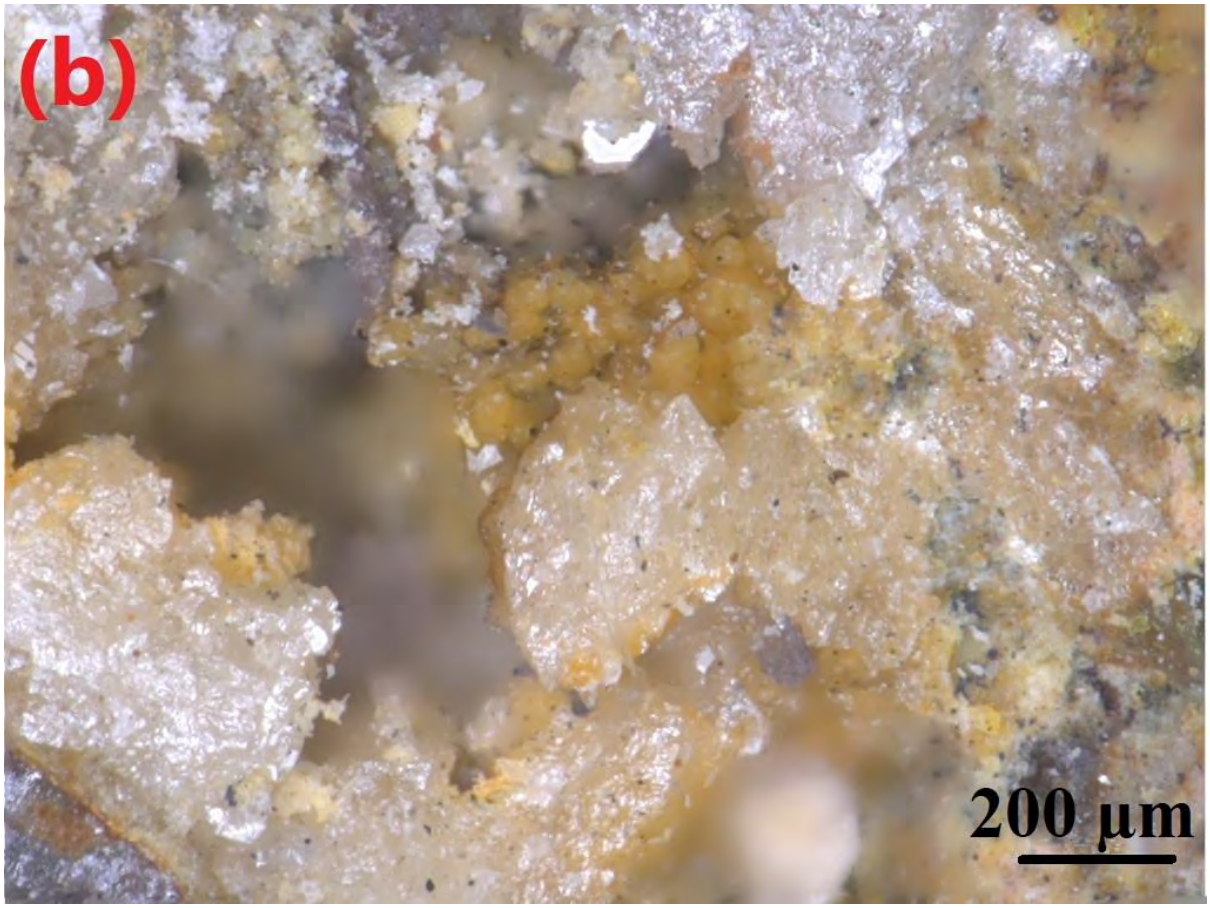

477

478

479 **Figure 4:** Images of the (a) 0*kl*, (b) *h*0*l*, and (c) *hk*0 layers showing very faint reflections
480 (labelled) indicating the presence of a larger unit cell (see text for details).

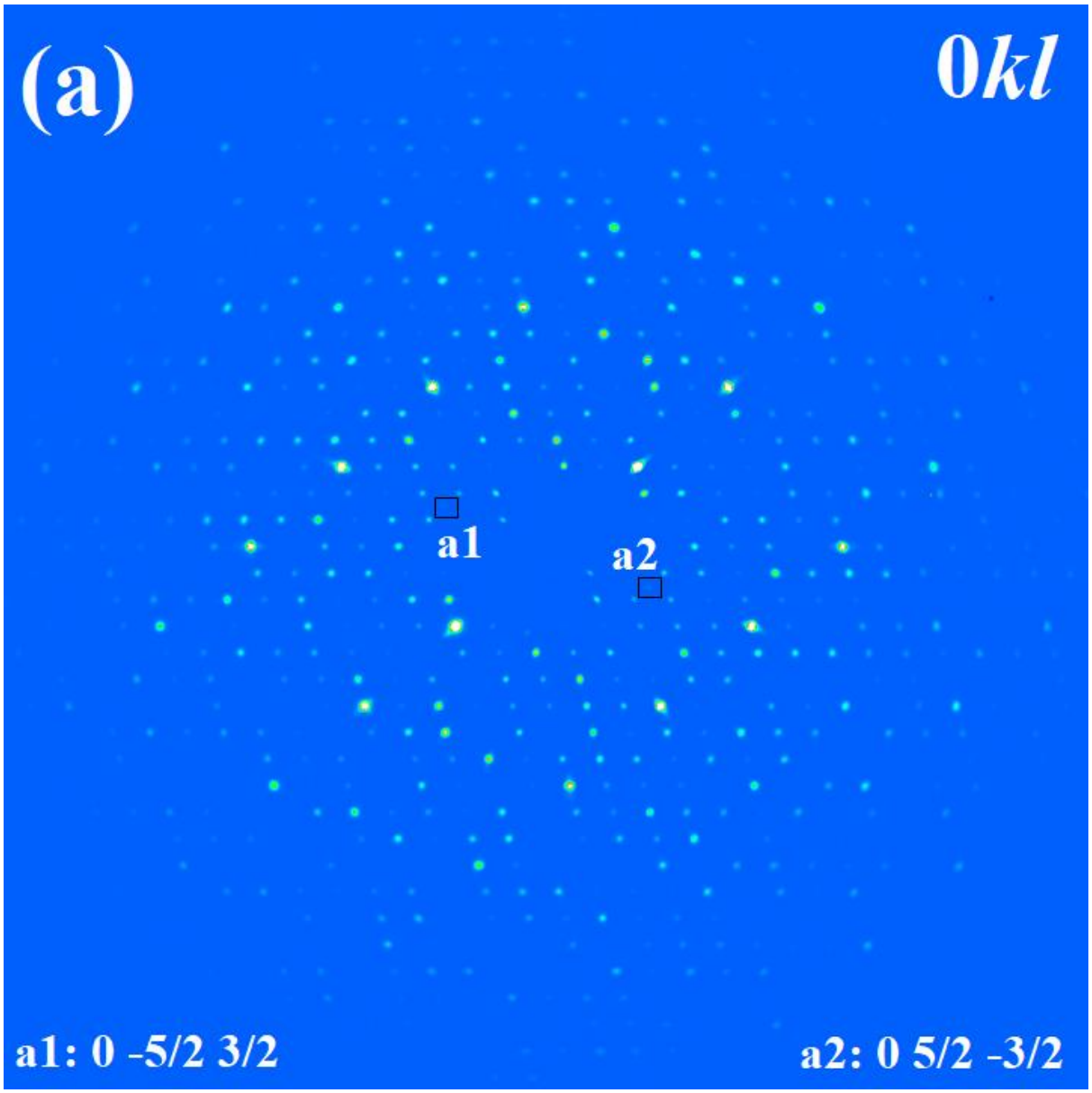

481

482

483

This is the peer-reviewed, final accepted version for American Mineralogist, published by the Mineralogical Society of America.
The published version is subject to change. Cite as Authors (Year) Title. American Mineralogist, in press.
DOI: https://doi.org/10.2138/am-2020-7536. http://www.minsocam.org/

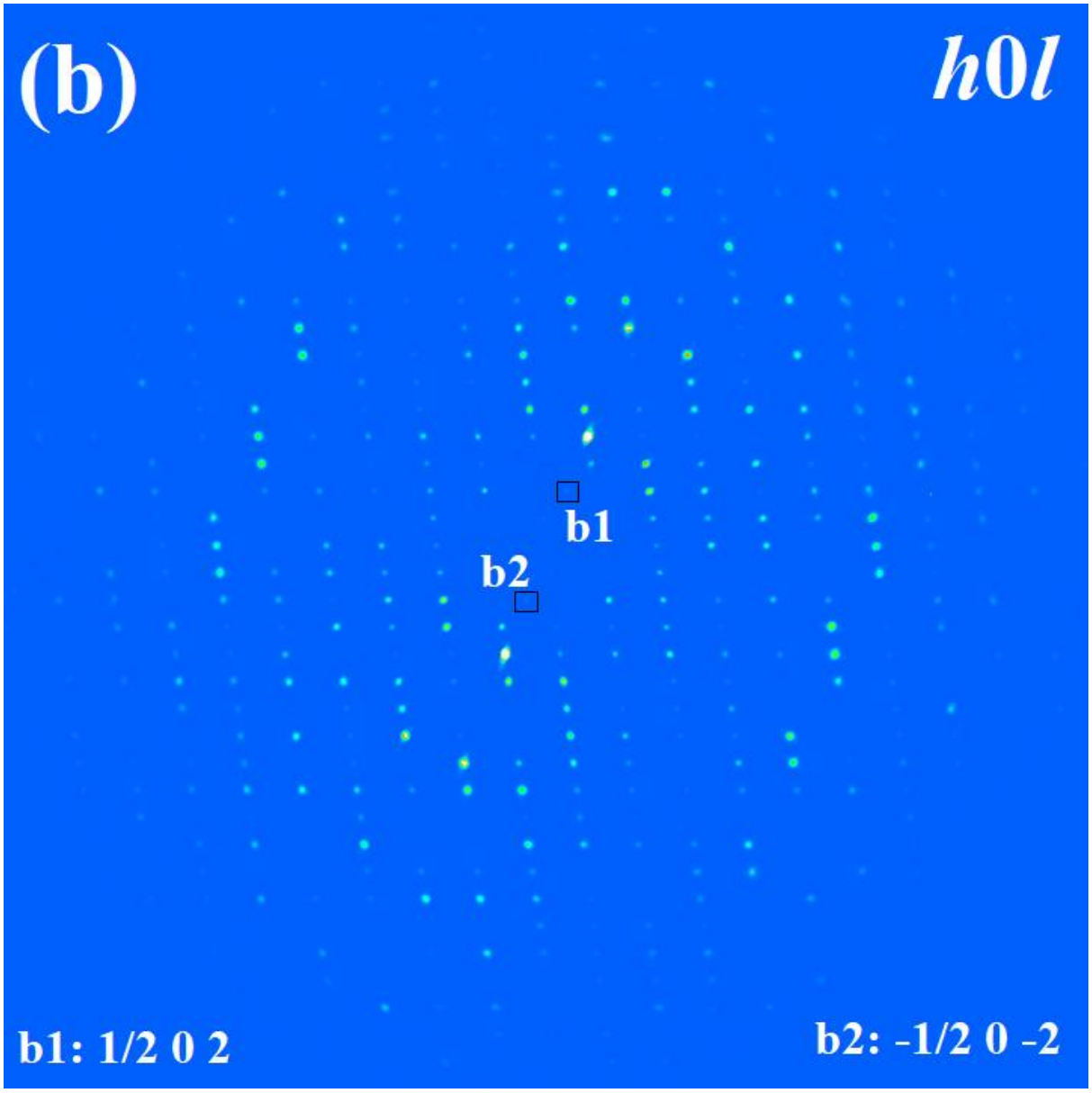

484

485

This is the peer-reviewed, final accepted version for American Mineralogist, published by the Mineralogical Society of America.
The published version is subject to change. Cite as Authors (Year) Title. American Mineralogist, in press.
DOI: https://doi.org/10.2138/am-2020-7536. http://www.minsocam.org/

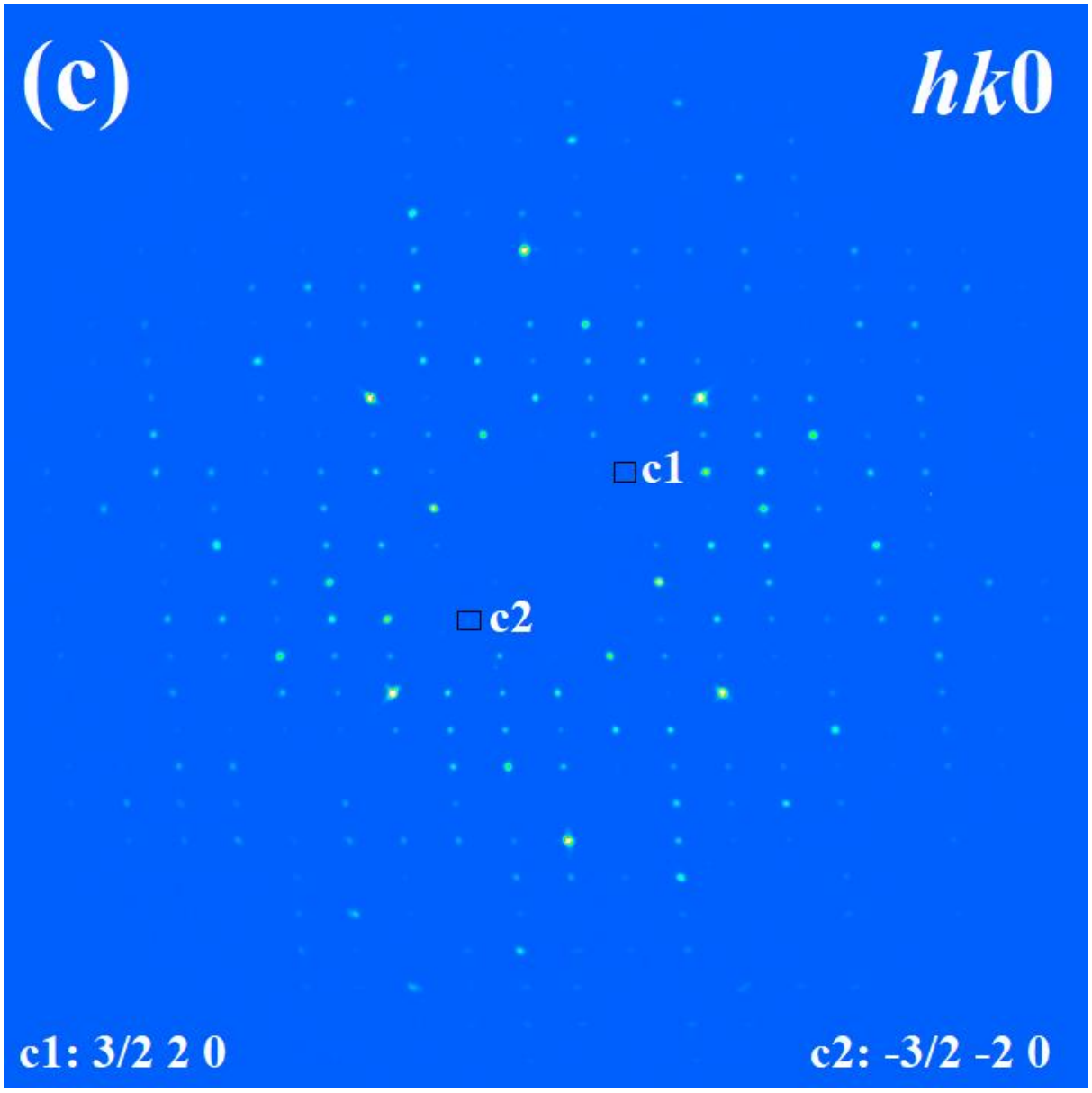

486

487

488 **Figure 5:** The crystal structure of fairbankite in a projection along the *a* axis, showing Pb atoms in grey, fully occupied $Te^{4+}O_n$ polyhedra (all
489 Te11/S1 shown as TeO_3) in dark green, and SO_4 tetrahedra (all S2/Te12 shown as SO_4) in yellow. $Te^{4+}O_n$ polyhedra are labelled by their Te site
490 number (1−11). The unit cell is outlined. This figure (and subsequent) drawn with Crystalmaker (2009).

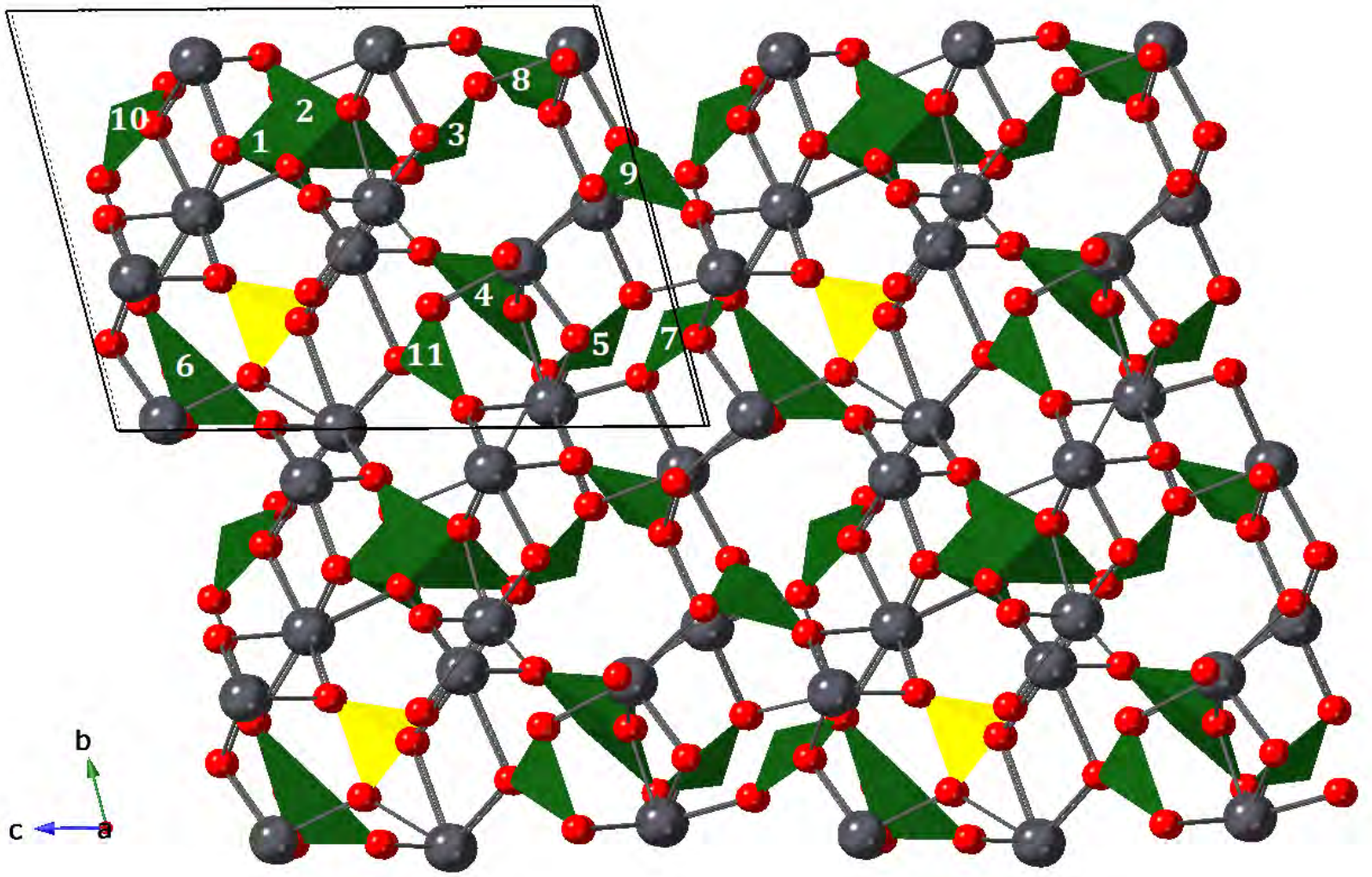

491

Figure 6: $Te^{4+}O_n$ polyhedra in fairbankite, with thick cylinders for primary and thin cylinders for secondary bonds. (a) *Soro* trimer comprised of $Te1^{4+}O_4$, $Te2^{4+}O_4$, and $Te3^{4+}O_3$, showing primary bonds only. (b) *Soro* dimer in polyhedral form as shown by $Te4^{4+}O_4$ and $Te5^{4+}O_3$ units. (c) *Soro* dimer (in ball-and-stick representation) as shown by $Te6^{4+}O_4$ and $Te7^{4+}O_3$ units. (d) Isolated $Te^{4+}O_3$ polyhedra as exemplified by Te8. Te9 and Te10 also form isolated trigonal pyramids.

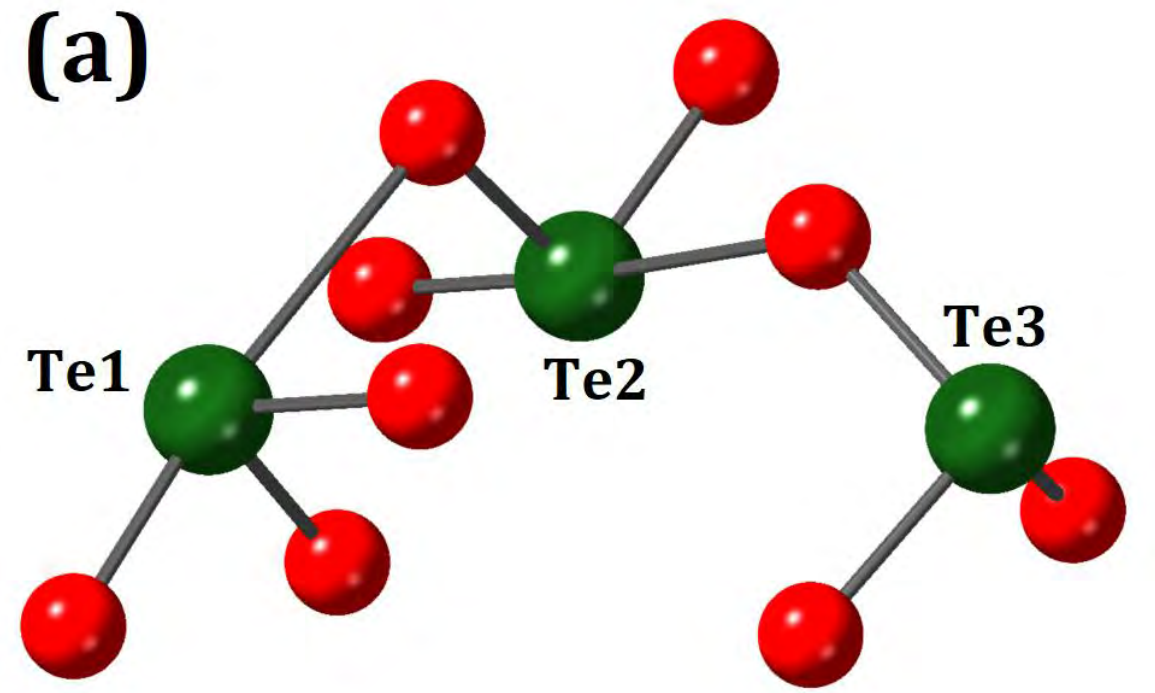

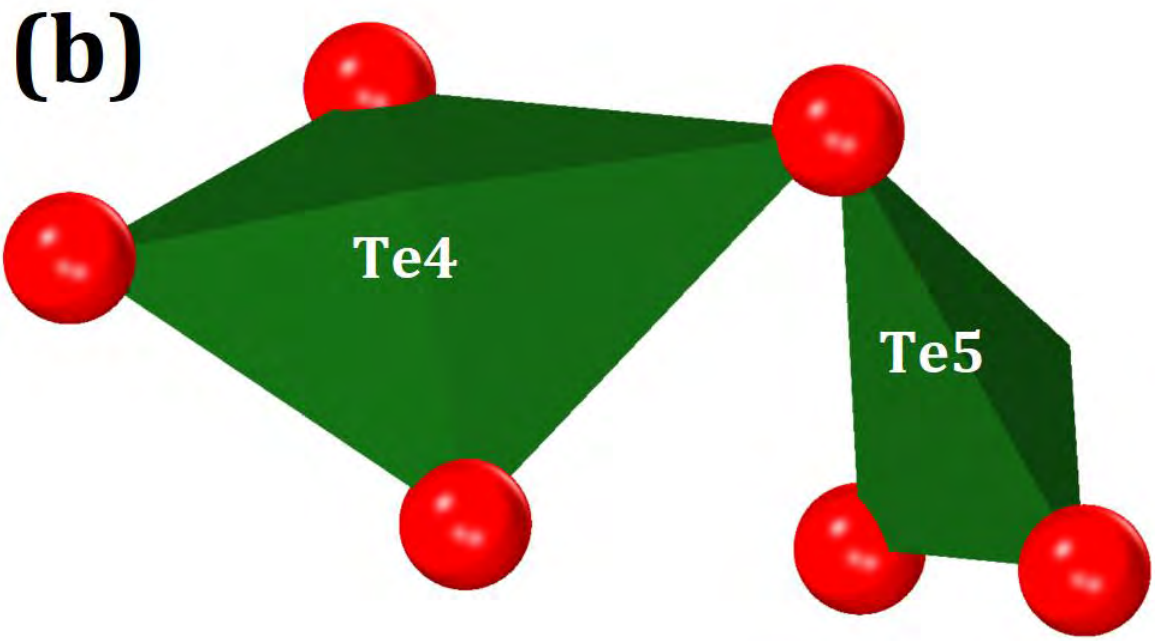

This is the peer-reviewed, final accepted version for American Mineralogist, published by the Mineralogical Society of America.
The published version is subject to change. Cite as Authors (Year) Title. American Mineralogist, in press.
DOI: https://doi.org/10.2138/am-2020-7536. http://www.minsocam.org/

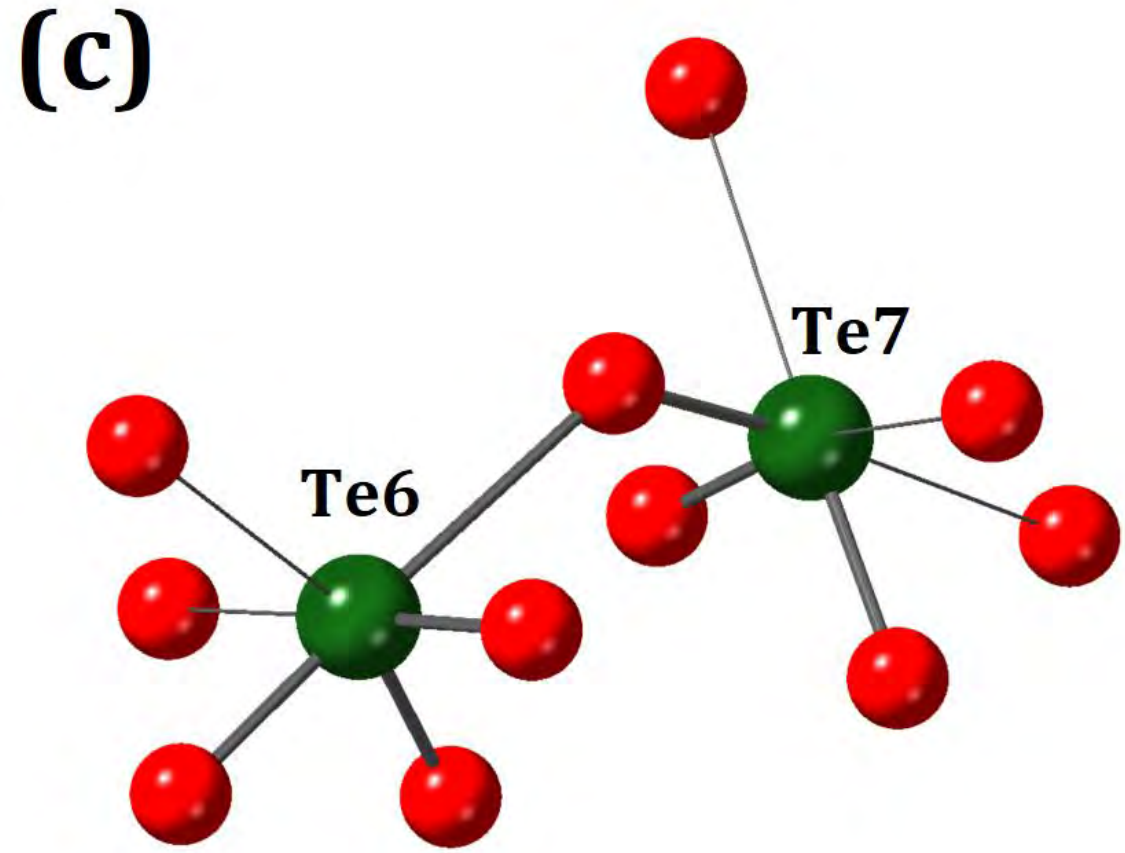

500

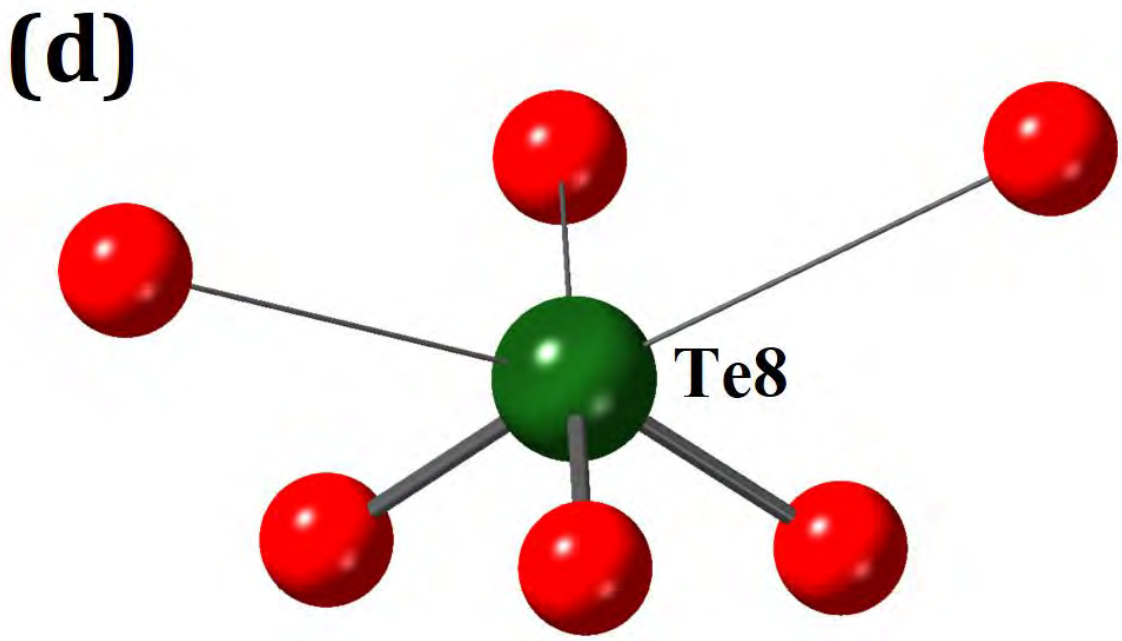

501

502 **Figure 7:** Representations of the two mixed Te/S sites, with bonds to O having an average
503 length between Te^{4+}–O bonds and S^{6+}–O bonds (closer to Te^{4+}–O average for the Te-
504 dominant Te11/S1 site, and closer to the S^{6+}–O average for S-dominant S2/Te12 site).

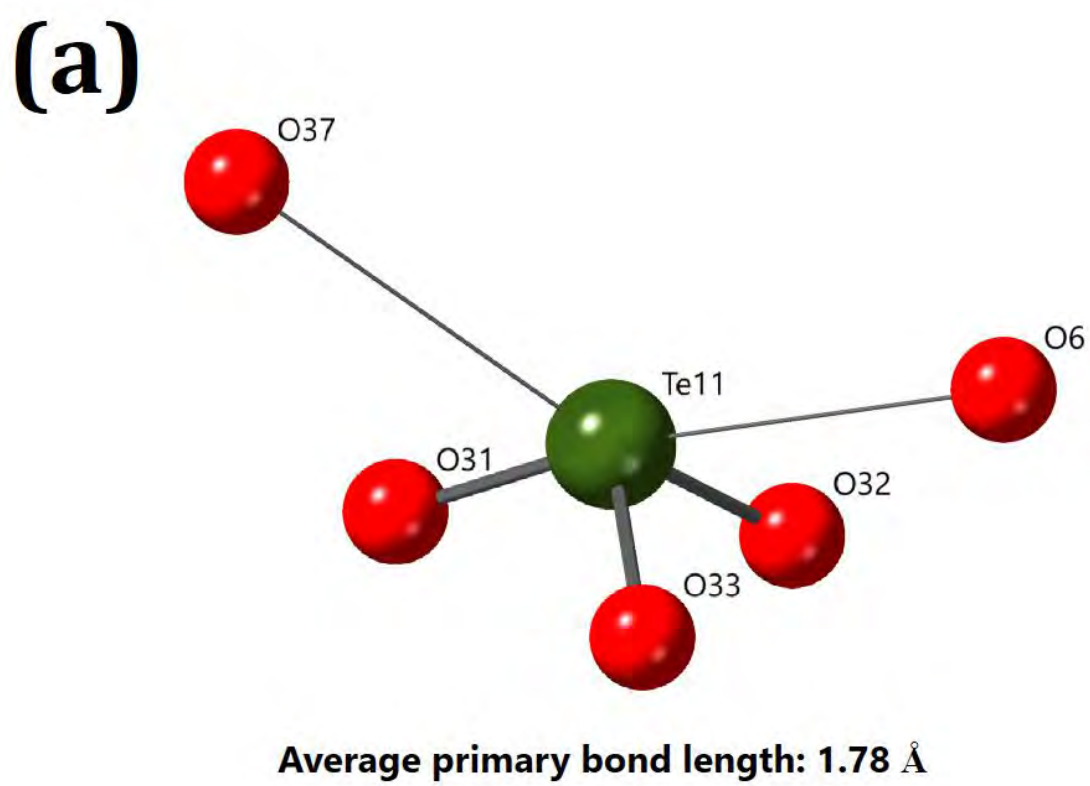

505

506